Evidence for Inhibitory Interaction of Hyaluronan-binding Protein 1 (HABP1/p32/gC1qR) with *Streptococcus pneumoniae* Hyaluronidase*

Gitanjali Yadav[‡1], **Ramachandra L. A. Prasad**[§], **Babal Kant Jha**[§], **Vivek Rai**[‡], **Vinod Bhakuni**[¶], and **Kasturi Datta**[§2]

From the ‡Computational Biology Laboratory, National Institute for Plant Genome Research, Aruna Asaf Ali Marg, New Delhi 110067, India, §Biochemistry Laboratory, School of Environmental Sciences, Jawaharlal Nehru University, New Delhi 110067, India, and ¶Division of Molecular and Structural Biology, Central Drug Research Institute, Lucknow 226001, India

Bacterial hyaluronan lyase enzymes are the major virulence factors that enable greater microbial ingress by cleaving hyaluronan (HA) polymers present predominantly in extracellular space of vertebrates. Based on the premise that effective inhibitors may bind to and stabilize HA thereby protecting it from degradation, here we investigated inhibitory activity of human hyaluronan-binding protein 1 (HABP1) on bacterial hyaluronidase because it is highly specific to HA and localized on the cell surface. Biochemical characterization revealed that HABP1 is a competitive inhibitor of *Streptococcus pneumoniae* hyaluronate lyase (SpnHL) with an IC_{50} value of 22 μM. This is thus the first report of an endogenous protein inhibitor that may be used during natural antibacterial defense. Our findings also support a novel multipronged mechanism for the high efficacy of HABP1-mediated inhibition based on structural modeling of enzyme, substrate, and inhibitor. Evidence from docking simulations and contact interface interactions showed that the inherent charge asymmetry of HABP1 plays a key role in the inhibitory activity. This novel role of HABP1 may pave the way for peptide inhibitors as alternatives to synthetic chemicals in antibacterial research.

Bacterial hyaluronidases have long been known as the "spreading factors" or virulence factors responsible for a wide range of acute and invasive infections in humans causing life-threatening diseases, such as pneumonia, meningitis, and septicemia among many others (1–3). These enzymes directly facilitate the spread of infection by degrading the HA[3] matrix, which constitutes a highly organized network in the extracellular space in all vertebrates, acting as a diffusion barrier *in vivo* and regulating the transport of other substances through the intercellular space (4). The HA matrix in extracellular matrix is mainly composed of HA polymer, a negatively charged polysaccharide of repeating disaccharide units of D-glucuronic acid (β-1,3) and *N*-acetyl-β-D-glucosamine, and is highly viscous in nature (5). Hyaluronidases are able to split this matrix, reducing its viscoelasticity and increasing membrane permeability, thereby allowing greater microbial access to or promoting diffusion between host tissues for colonization (4, 6, 7). The organized structure of HA substantially influences binding to receptors and to the active site of hyaluronidases. Bacterial hyaluronidases, isolated from strains of various microorganisms such as *Clostridium*, *Micrococcus*, *Streptococcus*, or *Streptomyces*, degrade HA at very fast rates via a β-elimination reaction that cleaves the alternate β-1,4-glycosidic linkage between the repeating units, resulting in unsaturated disaccharide products (8, 9). Although the mechanism of hyaluronidase-mediated degradation of HA has been very well elucidated through biochemical as well as structural investigations (10, 11), relatively little is known about the defense mechanisms used by the host during infection or about the role of HA and hyaluronidase in pathophysiological processes. It is believed that the balance of HA biosynthesis and intrinsic hyaluronidase levels may be regulated by invoking specific inhibitors (12–14). As a result, potent and specific inhibitors of bacterial hyaluronate lyase would have enormous therapeutic potential as drugs in the treatment of various bacterial infections.

The search for effective hyaluronidase inhibitors began more than half a century ago (2, 15–18) and continues to this day. Exogenous small molecule inhibitors have been identified, but they have weak potency and low selectivity, and there are many unanswered questions with regard to their mechanism of inhibition and whether they would be active against bacterial hyaluronidases as well. For example, heparins and derivatives of alginic acids (19, 20) have structural similarity to HA, whereas polyphenols, flavone analogues (21), saponins, norlignans, or antiallergic drugs are among other reported inhibitors of hyaluronidases (22, 23). Vitamin C, L-arginine derivatives, and fatty acids have been reported to inhibit streptococcal hyaluronidases at submillimolar concentrations, but a comparison of percent inhibition and IC_{50} values between these and previous reports is difficult because of differences in the experimental conditions (24–26). In view of the enormous medical applications of effective inhibitors, a systematic search has continued, using computer-aided drug design strategies. A rational analysis based on structural interactions led to the identification of a hydrophobic derivative of vitamin C as a strong inhibitor of

---

[3] The abbreviations used are: HA, hyaluronan; HABP1, hyaluronan-binding protein 1; SpnHL, *S. pneumoniae* hyaluronate lyase; a.s.a., accessible surface area.

Streptococcus agalactiae hyaluronidase, but it was weakly active against *Streptococcus pneumoniae*, a major human Gram-positive pathogen (27). Computer-aided drug design-based strategies mainly explore new leads by virtue of structural similarity to HA or, in some cases, by rational *de novo* approaches. An alternative strategy may also exist wherein an inhibitor may bind to and stabilize HA thereby protecting it from degradation. Such an alternative is plausible because HA has been known to bind and interact with receptors and a large number of HA-binding proteins. Hyaladherins are a very well characterized and highly selective family of proteins reported to interact non-covalently with HA and have a wide array of functions, including receptor-mediated activation of intracellular signaling and structural aggregations in the extracellular matrix (28–30). We therefore began this work with the surmise that a potent hyaluronidase inhibitor may be supplied endogenously by one of these ubiquitous proteins. HABP1 (synonym human p32 or gC1qR), a member of the multifunctional hyaladherin family, is a 68-kDa protein originally purified and cloned from human fibroblast as a novel HA receptor by our group (31). In this work, HABP1 was tested as an inhibitor of bacterial hyaluronidase because we had already confirmed its localization on the cell surface (32). According to the crystal structure of HABP1, it exists as a homotrimer having N-terminal α-helices and asymmetric charge distribution with structural plasticity (33).

Here we report the role of HABP1 as an inhibitor of *S. pneumoniae* hyaluronidase (SpnHL) and the elucidation of its competitive nature of inhibition. We also propose a unique multipronged mechanism of action based upon evidence from structural modeling of the interactions among substrate, enzyme, and inhibitor. Thus we present biochemical evidence for a novel role of HABP1 in pathophysiological processes as a highly potent inhibitor of SpnHL, offering a variety of avenues for optimization of selectivity and potency.

EXPERIMENTAL PROCEDURES

General Materials and Reagents—Substrate from human umbilical cord HA was purchased from Sigma Co. All other chemicals were of analytical grade and obtained from Sigma.

Purification and Estimation of HABP1—HABP1 (amino acids 74–282) was overexpressed in *Escherichia coli* and purified following the method described earlier (34) with modifications using the 55–90% ammonium sulfate cut followed by ion exchange chromatography on Mono Q^{TM} HR (10/10) column (Amersham Biosciences) using a linear gradient of 0–1 M NaCl in 20 mM Tris, pH 7.2, after washing the column with 150 mM NaCl in 20 mM Tris, pH 7.2. The pooled peak fractions were dialyzed in 150 mM NaCl, 20 mM Tris, pH 7.2, and quantified for further use.

Assay of SpnHL Enzymatic Activity—The activity of SpnHL was determined following the method described earlier (35) and is defined as its ability to break down HA to unsaturated disaccharide units (36). In a 1-ml solution of 0.2 mg/ml HA in 50 mM sodium acetate buffer, 10 mM CaCl$_2$, pH 6.5, 10 μl of enzyme sample (3 ng/μl, diluted just before taking measurement) was added. The reaction mixture was incubated for 5 min during which the measurements were carried out by monitoring the increase in absorbance at 232 nm at 25 °C in a Cary 100 Bio UV-visible double beam spectrophotometer (Varian Inc.).

Determination of Inhibitory Activity on Hyaluronidase—The *in vitro* enzyme inhibition experiments were performed with varying concentrations of HABP1. The inhibitory effect of HABP1 on *S. pneumoniae* hyaluronidase was measured by using two different enzymatic inhibition assays. In the first assay 0.2 mg/ml HA was preincubated with varying concentrations (0–100 μM) of HABP1 for 1 h at 4 °C in a l-ml reaction volume of 50 mM sodium acetate buffer, 10 mM CaCl$_2$, pH 6.5. The reaction was initiated with 30 ng of enzyme, and activity was measured. In the second assay, 30 ng of SpnHL was preincubated in the above mentioned 1-ml reaction volume of buffer with varying concentrations of HABP1 (0–100 μM) for 1 h at 4 °C. The reaction was initiated with 0.2 mg/ml HA, and enzymatic activity was measured. In both assays, the reaction was initiated exactly at 60 s after the addition of either enzyme or HA, respectively, to the reaction mixture. The progress of the reaction was monitored by detecting the appearance of HA oligosaccharide at 232 nm absorbance.

Enzyme Activity in Absence and Presence of Inhibitor—To study the effect of varying the concentration of substrate in the presence of inhibitor, HA concentration in solution was expressed as moles of hexasaccharide based on a hexasaccharide molecular weight of 1203.9 (37). In the absence of inhibitor, varying concentrations of HA (0.0625–0.750 mM) in 150 mM sodium acetate buffer, 10 mM CaCl$_2$, pH 6.5, was added to the enzyme (30 ng), and the activity was measured. In the presence of inhibitor, 20 μM HABP1 was preincubated with the enzyme (30 ng) for 1 h at 4 °C in a 1-ml reaction volume of buffer, increasing concentrations of HA (0.0625–0.750 mM) were added, and enzymatic activity was measured exactly 60 s after the HA was added to the reaction mixture. The progress of the reaction was monitored by detecting the appearance of HA oligosaccharide at 232 nm absorbance.

Initial Velocity Measurement and Data Analysis—The reaction progress curves for the enzymatic activity and enzyme inhibition were obtained by measurement of the absorbance at 232 nm due to the unsaturated disaccharide product. The reaction was carried out in a 1-ml solution of 50 mM sodium acetate buffer, 10 mM CaCl$_2$, pH 6.5, with substrate concentration ranging from 0.2072 to 0.3469 mM HA in the above buffer. The reaction was initiated by the addition of 10 μl of enzyme in the same buffer. The product absorbance was measured every 60 s for 5 min at 25 °C. The reaction progress was linear over the time of measurement within the precision of the instrument. The initial velocity of the reaction was determined from the increase in absorbance over the first 5 min of the reaction. The slope was divided by the molar absorption coefficient for the disaccharide product, 5.5×10^3 mol^{-1} cm^{-1} (36). The values were calculated and expressed in μM/min HA degradation by SpnHL in the presence of HABP1.

The data for initial velocity, V_i, from each experiment in which the concentration of substrate, S, was varied, were fit into the Michaelis-Menten equation with a nonlinear regression program (GraphPad Prism, version 5, GraphPad Software Inc., San Diego, CA). For all experiments, goodness-of-fit statistics showed that R^2 and correlation values were greater than 0.987

and 0.982, respectively. Among the curve fitting results, the program gave values of V_{max} and K_m as well as their respective standard deviations (σ).

Computational Simulations—The structural details of the interactions among substrate, enzyme, and inhibitor were elucidated by molecular docking experiments. Available crystal structures of the *S. pneumoniae* hyaluronate lyase (Protein Data Bank code 1LOH) and human HABP1 (Protein Data Bank code 1P32) were used for docking studies (33). The three-dimensional structures of the HA oligomers, namely disaccharide, tetrasaccharide, and hexasaccharide, were processed from the available crystal structure complex of SpnHL and HA hexasaccharide (Protein Data Bank code 1LOH). Details of local non-covalent interactions were studied using an in-house Fortran program/script that requires an interacting complex in Protein Data Bank format. The solvent-accessible area lost upon complexation was measured using NACCESS (38). All visualizations and renderings were done using VMD (Visual Molecular Dynamics) (39) and PyMOL (40).

Substrate Inhibitor Interaction—The three-dimensional structure of the inhibitor (Protein Data Bank code 1P32) having three potential active sites (one per monomer) was treated as the static "receptor" molecule with HA polysaccharide as the mobile "ligand" molecule. The three processed HA oligomers were docked to HABP1, one at a time, with the experimentally characterized BX_7B (where *B* is a basic residue) HA binding motif (residues 119–128, 1P32 numbering) defined as the binding site (31, 41). Flex-X molecular docking program was used because it is able to accurately predict the geometry of the protein-ligand complex for a protein with known three-dimensional structure and a small ligand molecule. Flex-X is based on a robust incremental construction algorithm where the ligand is decomposed into pieces and thereafter flexibly rebuilt in the active site using multiple placement strategies followed by a ranking of all orientations using a variety of scoring functions. Hydrogens were added to both structures before the experiment. Default parameter values were used, and the top ranking orientations were considered for further analysis.

Enzyme Inhibitor Interaction—The enzyme *S. pneumoniae* hyaluronate lyase protein (Protein Data Bank code 1LOH), which was the smaller of the two proteins, was kept flexible and docked onto the HABP1 homotrimer, which was kept static. Preprocessing of the hyaluronidase involved removal of HA and water molecules. The receptor and ligand were projected onto a 160-Å cubical grid using ZDOCK, a rigid body docking program, followed by a refinement program, RDOCK. ZDOCK uses a fast Fourier transform to search all possible binding modes for the proteins, evaluating based on shape complementarity, desolvation energy, and electrostatics. The top 2000 predictions from ZDOCK were submitted to RDOCK where they were minimized by CHARMM (Chemistry at Harvard Molecular Mechanics) to improve the energies and eliminate clashes. Finally the electrostatic and desolvation energies were recomputed by RDOCK, and the top ranking complex was selected for analysis of the contact interface.
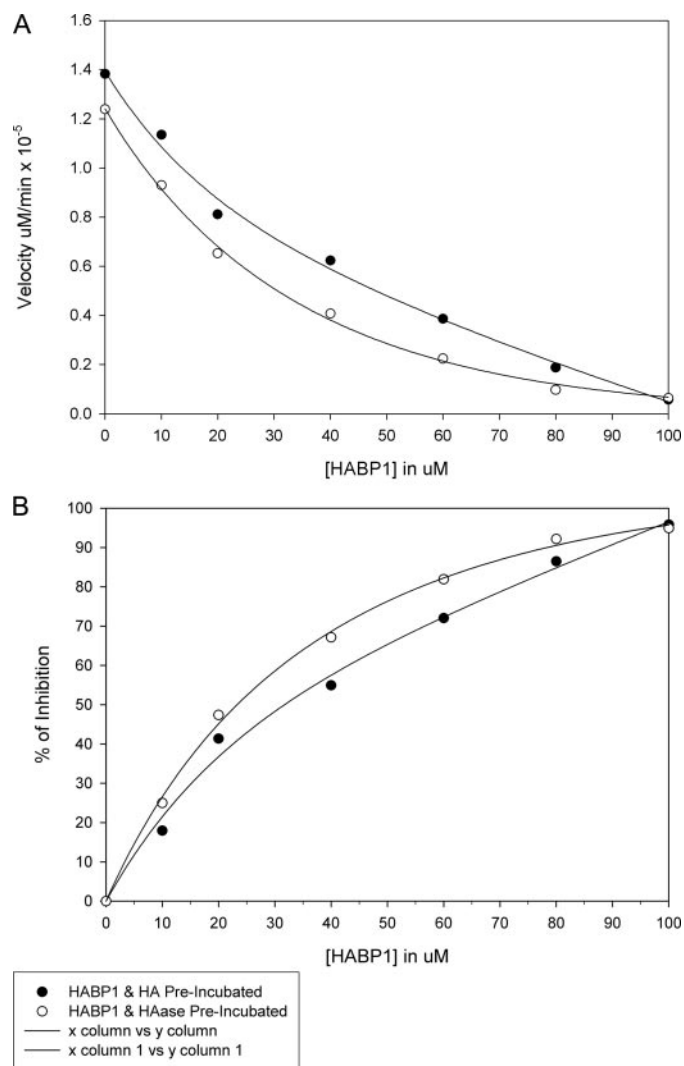

FIGURE 1. **Inhibition of SpnHL activity by HABP1 in a concentration-dependent manner.** In *A*, the graph represents the inhibition of SpnHL activity with increasing concentration of HABP1 as described under "Experimental Procedures." The first curve (●) represents HA preincubated with increasing concentrations of HABP1 (0–100 μM) before the reaction was initiated with 30 ng of the enzyme. The second curve (○) represents increasing concentrations of HABP1 (0–100 μM) preincubated with SpnHL (10 μl of 3 ng/μl) before the reaction was initiated with 0.2 mg/ml HA. In both cases, activity was measured at 232 nm. In *B*, the graph represents the percent inhibition of SpnHL activity as plotted against varying concentrations of inhibitor. The values represent the average of four different experiments.

RESULTS

In Vitro Effect of HABP1 on the Activity of SpnHL

The *in vitro* enzyme inhibition experiments demonstrated that highly purified HABP1 inhibits SpnHL activity in a concentration-dependent manner as shown in Fig. 1. The activity of purified SpnHL gradually decreased in the presence of increasing concentrations of purified HABP1 either when HABP1 was preincubated with HA and the reaction was initiated with SpnHL or when it was preincubated with the enzyme SpnHL and the reaction was initiated with HA. This can be seen much better in Fig. 1*B*, which shows a plot of percent inhibition of SpnHL activity *versus* inhibitor concentration. HABP1 was found to inhibit SpnHL with an IC_{50} value of 22 μM.
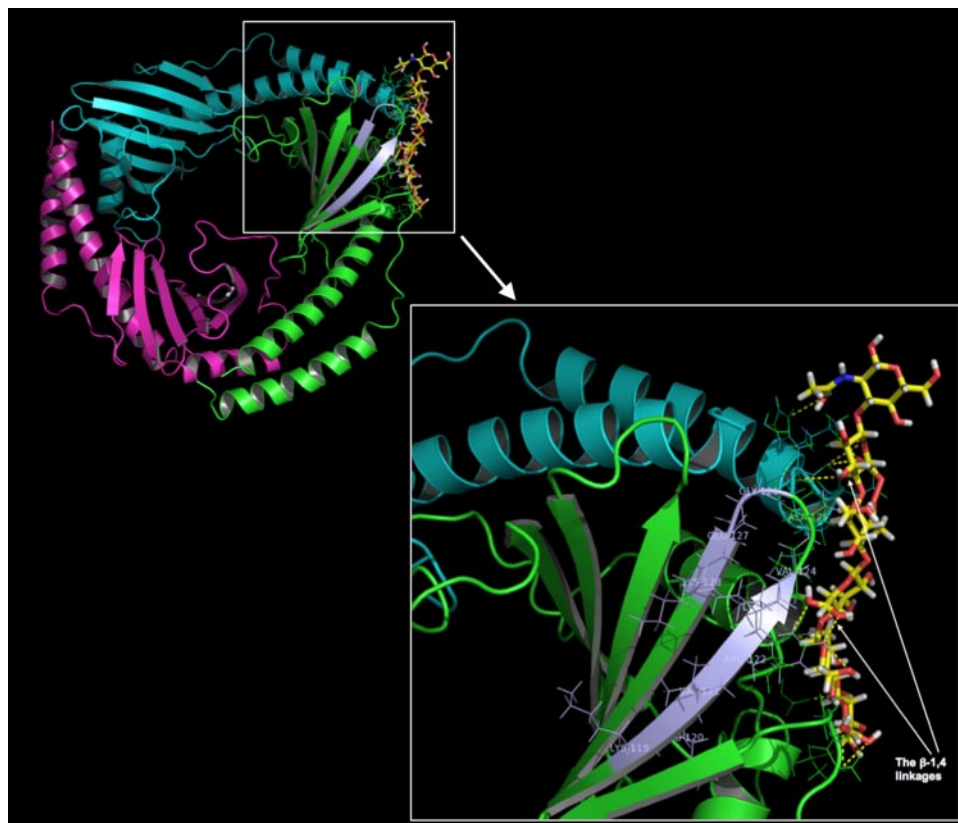
FIGURE 2. **Model of hyaluronan binding by HABP1.** Each monomer of the HABP1 trimer has been shown in distinct colors. The docked complex depicts HA hexamer (shown in atom colors) closely bound to one of the HA binding motifs (depicted in *gray*) on the trimeric HABP1 protein. The *inset* zooms into the complex to show the details of the contact interface between the ligand and receptor. Hydrogen bonds are depicted as *yellow dashes*. As can be seen, the β-1,4-glycosidic linkage is protected during binding, being tethered by hydrogen bonds and hydrophobic interaction on all sides.

chains. The hexasaccharide sugar was found to bind with HABP1 strongly via hydrophobic as well as hydrogen bond interactions. Interestingly the two β-1,4-glycosidic linkages of the HA polymer (one between HA1 and HA2 and the other between HA2 and HA3) are both entirely buried in this complex; they are tethered on both sides by hydrogen bonds as well as hydrophobic interactions. For example, the C-1 and C-4 carbon atoms that mediate the β-1,4-glycosidic linkages are bound by multiple hydrophobic interactions with HABP1 residues His-75 and Thr-76 for the first linkage and Asp-245, Arg-246, and Gly-247 for the second linkage. Furthermore residue Arg-122 of the HA binding motif plays a key role in the first linkage, making hydrogen bonds with the glucuronate moiety on the sugar preceding the linkage and the secondary alcohol group on the sugar succeeding the linkage. Motif residues Arg-122 and Ala-125 also participate in hydrophobic interactions with the ligand. The binding between HABP1 and the HA hexasaccharide is further strengthened by side chains of Lys-80, Ser-106, and Arg-244 that make hydrogen bonds with the sugar and Met-74, Gly-107, Asp-249, and Thr-251 that are involved in hydrophobic interactions. Atomic details of the all these interactions have been provided in Table 1.

Thus the collective strength of a substantial number of noncovalent interactions at the contact interface enhances the binding of HA oligomers to HABP1, thereby protecting HA from degradation. It may be noted that the inhibitor is in the homotrimeric form, and the interaction causes a very small loss of accessible surface area (479 Å^2; roughly 2% of the entire molecule) at one of the three interchain junctions (see Fig. 2). Therefore it is plausible that the remaining two interchain junctions of HABP1 could potentially bind more HA molecules, or a much longer HA polymer may utilize all three binding sites at various regions along its length, ensuring protection.

Structural Modeling: Binding of HA Hexasaccharide to HABP1

It has been reported that the alternate β-1,4-glycosidic linkage within HA gets cleaved by SpnHL (37), and we were interested in finding out whether HABP1 mediates SpnHL inhibition by protecting this bond during its interaction with HA. To test this, we structurally modeled the HABP1 and HA interaction. The results showed that binding of HA to HABP1 indeed involves the β-1,4-glycosidic linkage site on the HA oligomer, explaining the observed reduction in enzyme activity.

Docking simulations depicted a steric fit between substrate and inhibitor. Interestingly when the top ranking orientations were analyzed to elucidate the molecular details of binding, the HA hexasaccharide was predicted to bind with an energy of −7.59 kcal/mol, whereas the tetrasaccharide and disaccharide HA oligomers showed binding energies of −6.56 and −6.28 kcal/mol, respectively. These observations are in agreement with previous experimental reports stating that the HA hexasaccharide shows better binding affinity than its shorter oligomers (42). Fig. 2 shows the top ranking confirmation between the hexasaccharide substrate and inhibitor after refinement as described under "Experimental Procedures." A total of 24 contacts were observed between the sugar and HABP1 of which 17 were from chain A and seven were from chain B. Thus, only two of the three polypeptide chains of HABP1 participate in this interaction, and binding occurs at the junction of these two

Competitive Nature of SpnHL Inhibition by HABP1

To determine the nature of inhibition observed during the preincubation of SpnHL and HABP1 (Fig. 1), enzyme assays were carried out either in the absence or in the presence of purified HABP1 (20 μM). Fig. 3 depicts the plot of substrate concentrations against the enzyme activity in the presence and absence of inhibitor. An inhibition of 20–30% was observed in the presence of the inhibitor. The plot shows that reaction was linear over the time of measurement, and the initial velocity and

TABLE 1

Interactions and surface accessibility at the HABP1-HA hexasaccharide contact interface

For each HA unit, UA and NAc denote β-D-glucuronic acid and *N*-acetyl-β-D-glucosamine, respectively. Stars (**) mark the C-1 and C-4 atoms that participate in the two crucial β-1,4-glycosidic linkages present in the HA hexasaccharide. Distance, distance in Å between interacting atoms from sugar and HABP1. RSA δ (HA) is the loss in residue surface accessibility (RSA) of HABP1 residues upon complexation with HA measured in Å^2. "Hyp" denotes a hydrophobic interaction. RSA δ (HL) shows the partial a.s.a. lost from three residues of one chain of the HABP1 trimer during SpnHL inhibition. The last three rows depict residues that lose accessibility but do not directly interact with the sugar. HA1, HA2, and HA3 denote the three hyaluronan units of the hexasaccharide. chn, chain; res, residue; id, identity; na, not applicable.

| HA	HA Sugar	chn	res id	atom	Distance (Å)	RSA δ (HA)	Interaction	RSA δ (HL)
UA of HA1								
C	glucuronate CO₂	A	106 SER	CB	3.53	31.92	hyp	none
C2		A	251 THR	CB	3.69	33.21	hyp	none
C2		A	251 THR	CG2	3.493	"	hyp	none
C3		A	251 THR	CB	3.986	"	hyp	none
C35	C1 atom	A	249 ASP	CG	3.697	38.49	hyp	2.81
H41		A	249 ASP	OD1	1.789	"	H- bond	"
NAc of HA1								
8H2	CH₂OH group	A	122 ARG	NH2	2.052	34.29	H- bond	none
C26	Acetyl group	A	244 ALA	C	3.774	25.76	hyp	6.72
C27	CH₂OH group	A	107 GLY	CA	3.396	21.76	hyp	none
C27		A	122 ARG	CZ	3.282	34.29	hyp	none
C28		A	122 ARG	CZ	3.892	"	hyp	none
C28		A	247 GLY	CA	3.171	23.42	hyp	none
C29		A	247 GLY	CA	3.91	"	hyp	none
C30	C3 atom	A	247 GLY	CA	3.538	"	hyp	none
C31		A	247 GLY	CA	3.802	"	hyp	none
C32	C1 atom **	A	245 ASP	C	3.648	38.68	hyp	11.45
C32	" **	A	246 ARG	C	3.61	na	hyp	none
C32	" **	A	247 GLY	CA	3.07	23.42	hyp	none
C33		A	244 ALA	C	3.626	25.76	hyp	6.72
C33		A	244 ALA	CB	3.694	"	hyp	"
H38	NH₂ group	A	244 ALA	O	1.283	"	H- bond	"
H52		A	247 GLY	N	1.685	23.42	H- bond	none
UA of HA2								
C38		A	245 ASP	C	3.989	38.68	hyp	11.45
C38		A	245 ASP	CA	3.804	"	hyp	"
C39	C4 atom **	A	245 ASP	C	3.642	"	hyp	"
C40		A	245 ASP	C	3.664	"	hyp	"
H55		A	245 ASP	O	1.644	"	H- bond	"
O6A	glucuronate CO₂	B	80 LYS	3HZ	1.245	30.92	H- bond	none
O6A	"	A	106 SER	HG	2.244	31.92	H- bond	none
O6A	"	A	122 ARG	1HH2	1.863	34.29	H- bond	none
O6B	"	A	122 ARG	1HH1	2.127	"	H- bond	none
NAc of HA2								
C10	HA2	B	74 MET	CG	3.93	39.09	hyp	none
C11	C1 atom **	B	76 THR	CA	3.858	36.01	hyp	none
C11	" **	B	76 THR	CG2	3.585	"	hyp	none
C12		B	76 THR	CG2	3.724	"	hyp	none
C13	C3 atom	B	76 THR	CG2	3.782	"	hyp	none
C7	Acetyl group	B	76 THR	CA	3.704	"	hyp	none
C7	"	B	76 THR	CB	3.708	"	hyp	none
C7	"	B	76 THR	CG2	3.903	"	hyp	none
C8	CH₂OH group	B	74 MET	CG	3.318	39.09	hyp	none
C8	"	A	125 ALA	CB	3.372	20.33	hyp	none
C9		B	74 MET	CB	3.643	39.09	hyp	none
C9		B	74 MET	CG	3.102	"	hyp	none
UA of HA3								
C14		B	75 HIS	C	3.875	49	hyp	none
C23		B	75 HIS	C	3.997	"	hyp	none
C23		B	75 HIS	CB	3.618	"	hyp	none
C4	Acetyl group	B	76 THR	C	3.904	36.01	hyp	none
C4	"	B	76 THR	CA	3.944	"	hyp	none
C6	C4 atom **	B	75 HIS	C	3.162	49	hyp	none
C6	" **	B	76 THR	CA	3.723	36.01	hyp	none
H14		B	75 HIS	O	1.488	49	H- bond	none
O6	OH group	B	75 HIS	H	2.182	"	H- bond	none
na		B	77 ASP	na	na	31.89	none	none
na		A	109 TRP	na	na	1.2	none	none
na		A	124 VAL	na	na	4.43	none	none
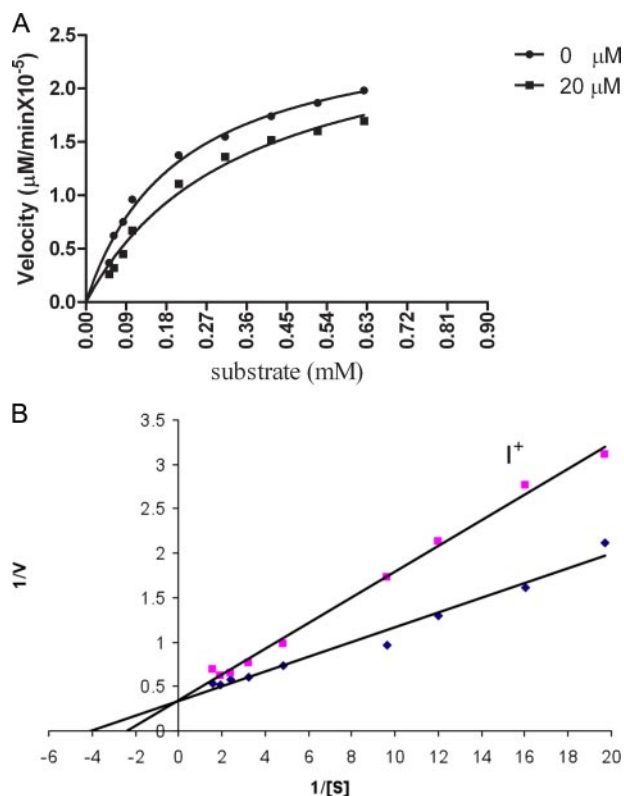
FIGURE 3. **Lineweaver-Burke plot representing competitive nature of inhibition.** *A*, Michaelis-Menten graph. *B*, Lineweaver-Burke plot. In both cases, *curve* ○ represents enzyme activity in the absence of HABP1 (0 μM), and *curve* ▲ represents 20–30% inhibition of enzyme activity in the presence of HABP1 (20 μM). The K_m and V_{max} values were calculated according to the Lineweaver-Burke plot. Each plot is representative of at least more than four separate experiments. The K_m was calculated to be 0.2765 and 0.41129 mM in the absence and presence of the inhibitor, respectively. The inhibitor inhibits the enzyme at a K_i value of 34.24 μM.

other parameters were calculated as described under "Experimental Procedures." The K_m was calculated to be 0.2765 and 0.41129 mM in the absence and presence of the inhibitor, respectively. A Lineweaver-Burke plot (double reciprocal) of the data obtained was indicative of competitive inhibition. The value for K_i was obtained from plots of $1/V$ versus $1/[S]$. It was found that HABP1 inhibits the enzyme at a K_i value of 34.24 μM. These results confirmed that the inhibition observed in Fig. 1 is competitive in nature.

Structural Modeling: Inhibition of Hyaluronidase Mediated by HABP1

To comprehend the molecular details and structural implications of the observed competitive inhibition, HABP1 was docked with SpnHL as described under "Experimental Procedures." Analysis of the top ranking docking complex confirmed that HABP1 binds to the enzyme in the same region where substrate HA has been reported to bind (37); the data thus support the competitive inhibition observed in the experimental assays.

Fig. 4*A* depicts the overall mode of binding with the *inset* (Fig. 4*B*) showing the molecular details of the interaction. An accessible surface area (a.s.a.) of ~2938 Å^2 (roughly 11% of the total a.s.a.) is buried on the negatively charged face of HABP1 trimer upon binding to SpnHL, occluding an a.s.a. of 5489 Å^2 (roughly
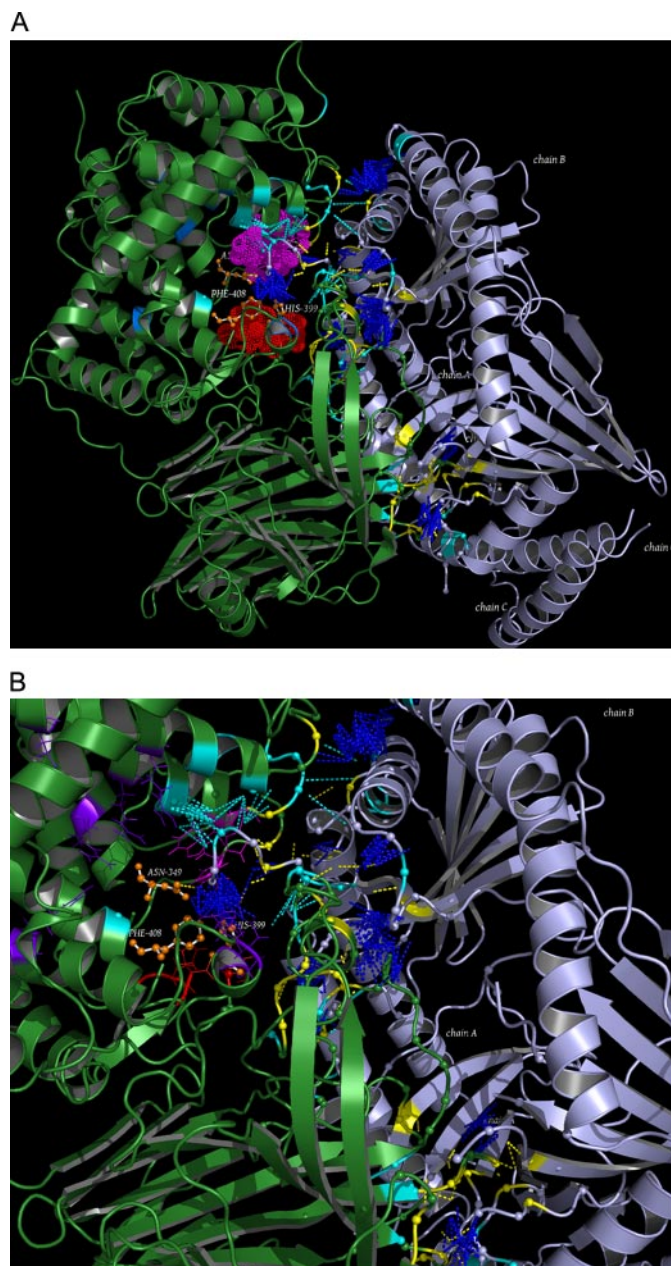
FIGURE 4. **HABP1 binding to SpnHL.** The enzyme SpnHL (*green* schematic) is shown docked with the inhibitor HABP1 (trimer shown in *silver* schematic). The active site is in the α-domain of the enzyme; catalytic triad residues have been labeled and depicted in *orange ball-and-stick* model. Residues of the aromatic patch can be seen in *pink* (*dots* in *A* and *lines* in *B*); the negative patch in the active site is depicted in *red* (*dots* in *A* and *lines* in *B*). Non-covalent interactions all along the contact interface are represented as *dashed lines* of distinct colors, namely hydrogen bonds (*yellow*), electrostatic interactions (*blue*), and hydrophobic interactions (*cyan*). Residues of both molecules involved in these interactions are colored in the same color as the interaction. (Only main chain carbon atoms are shown to maintain clarity.) As can be seen, most of the interactions are electrostatic in nature. *B* is an enlarged *inset* of *A*. Details are provided in the text.

20% of total a.s.a.) from the enzyme around its active site cleft. The majority of interactions at the contact interface emerge from the juxtaposition of these two large and oppositely charged surfaces. All three monomers of the inhibitor participate in binding. The refined model of binding revealed a total of 207 contacts between the two structures mediated by 49 residues from HABP1 and 81 residues from SpnHL. Of these, 25 are

ionic interactions. The inhibitory activity of HABP1 is evidently due to the combined effect of the considerable number of non-covalent interactions it forms with catalytically essential residues in the active site of the enzyme.

As can be seen in Fig. 4, the binding potency of the inhibitor is a virtue of electrostatic, hydrophobic, and hydrogen bonding interactions all along the contact interface mainly in the catalytic pocket region and a few involving the α-domain of the enzyme. Several interesting features of the complex become evident because the orientation of inhibitor obstructs the region on the enzyme where substrate must enter and bind, thereby rendering the cleft inaccessible. The majority of interactions at the interface are electrostatic in nature. It may be noted that the enzyme active site, which is in the form of a cleft between the two structural domains of SpnHL, has a highly positive center, and the negatively charged projection of HABP1 plays a key role in facilitating the attachment, thereby effecting the high charge complementarity at the interface. The maximum ionic contacts are observed in the product release region, which has previously been shown to be an important target site for hyaluronidase inhibitors (27). Small molecule-based inhibitor design strategies also target specific residues within the active site that are known to be crucial for catalysis. Targeting of these sites in the enzyme has been reported to add to the potency of inhibition (43). These reports add strength to our data because many of the reported crucial groups of residues were observed to be blocked by the inhibitor HABP1 in the final refined model as follows.

The Catalytic Triad—The side chain of the catalytically active His-399 residue is blocked by close proximity to the backbone and negative side chains of residue Asp-197 on the inhibitor. As shown in Fig. 4, residues His-399 and Asn-349 of the catalytic triad make electrostatic and hydrogen bond interactions with the inhibitor. His-399 makes a hydrogen bond with Ser-201 of HABP1, whereas Asn-349 is involved in hydrogen bonding with residue Asp-197. Although Tyr-408 does not interact specifically with the inhibitor, it is within 5-Å distance of the negative projection of HABP1 and thus rendered solvent-inaccessible.

The Aromatic Patch—Residues Trp-291, Trp-292, and Phe-343 of SpnHL are known to constitute the aromatic patch on one end of the enzyme cleft, which has been reported to be responsible for the correct positioning of substrate chains for catalysis, *i.e.* for the selection of cleavage sites on the HA substrate (27). Asp-197 of HABP1 completely obstructs this aromatic patch, making hydrophobic interactions with all three patch residues. Trp-292 makes additional hydrophobic interactions with residues 198–200 of the inhibitor. Interactions between other residues in the vicinity, namely Ile-296 and Gly-297 from the enzyme and Ala-199 from the inhibitor, further obstruct the surface accessibility of this patch. Overall these interactions lead to a total loss of more than 75% residue surface accessibility for the aromatic patch, thereby burying it extensively.

The Positive and Negative Patches—The dense electrostatic interactions at the binding interface depicted in Fig. 4 are formed between the outermost residues of the catalytically essential positive patch of the enzyme and the negative surface

of the inhibitor. For example, arginines 462 and 466 of this patch lose 27 and 47 Å^2 of their residue surface accessibility, respectively, to ionic interactions with glutamates 198 and 200 of HABP1, amounting to a 77.4% loss of accessibility. Other residues comprising the positive patch, namely Lys-250, Arg-300, Arg-355, and Arg-480, also get buried during the inhibitory interaction, resulting in an overall loss of 71% surface accessible area for this patch. The negative patch comprising residues Glu-388, Asp-398, and Thr-400 has been implicated in the product release process of SpnHL. The above mentioned interactions involving the positive patch of the enzyme also lead to the occlusion of the residues in the negative patch because the two patches lie in close vicinity of each other. In particular, Glu-388 was observed to lose 12.5-Å^2 (roughly 26%) surface area during the interaction with HABP1.

It may be noted that the residues of the HA binding motif (of HABP1) are not involved in any of its interactions with SpnHL. Of the three potential HA binding sites on a given HABP1 trimer, two are completely accessible during the inhibitory interaction. The third binding site shows a small overlap as three of the 24 HABP1 residues required for sugar binding lose partial side chain accessibility during the inhibitory interaction. These three residues are shown in Table 1. A perusal of this partially buried region reveals that the lost a.s.a. is relatively insignificant (roughly 6%) as a result of which all three binding sites of HABP1 retain sufficient accessibility when it mediates the inhibition of SpnHL. The significance of this observation for the mechanism of action is discussed below.

DISCUSSION

In the present study, we have characterized human HABP1 as the only known endogenous protein inhibitor of SpnHL, thus implying indirectly its functional role in defense against bacterial invasion. The mechanistic/structural aspects of this inhibition have been elucidated with the help of docking simulations. HABP1 with an IC$_{50}$ value of 22 μM is one of the most potent inhibitors of SpnHL reported to date. Ascorbic acid 6-hexadecanoate has previously been reported as an inhibitor of *S. agalactiae* hyaluronate lyase with an IC$_{50}$ of 4 μM, but it showed much weaker inhibition of SpnHL with an IC$_{50}$ of 100 μM (27). We have analyzed enzyme substrate interaction in context with enzyme-inhibitor and substrate-inhibitor interactions to elucidate the structural details of the observed inhibition.

Preincubation of HABP1 and HA was able to inhibit the enzyme activity, and there was no further degradation of HA upon addition of SpnHL to the reaction solution. It was observed that HA degradation and product release are totally dependent on the ratio of HABP1 and HA molecules present in the reaction solution. With the increase in HABP1 concentration in the reaction solution, a decrease in enzymatic activity was observed, whereas upon increasing the concentration of HA, the enzymatic activity was retained. For a given amount of HA, however, low HABP1 was not able to block enzyme or sequester substrate, but with high concentration of HABP1, 95% inhibition was observed. Furthermore there was no change in enzymatic activity when the concentration of HA was kept equal to that of HABP1. It is therefore plausible that during the preincubation binding occurred between HABP1 and its ligand

HA, thereby protecting the latter from the enzyme. This deduction was structurally supported by docking experiments between HABP1 and HA that revealed a tight binding with the β-1,4-glycosidic linkage of HA via hydrogen bonding as well as hydrophobic interactions (shown in Fig. 2 and Table 1).

Having thus confirmed the protection of HA by HABP1, we tested whether this was the exclusive mode of inhibition used by the inhibitor. As shown in Fig. 1*A*, the inhibition of enzyme observed upon preincubating substrate and inhibitor was found to be comparable to the inhibition observed upon preincubating the enzyme and inhibitor. Subsequently assays were carried out to determine the nature of this inhibition. As shown in Fig. 3, Lineweaver-Burke plot analysis confirmed that HABP1 inhibits SpnHL activity in a competitive manner. Docking experiments between SpnHL and HABP1 further provided the molecular details of the contact interface between HABP1 and the active site cleft of SpnHL (Fig. 4). It was also observed that HABP1 uses only the negative side/face of its trimeric (roughly flat) structure during the inhibition of SpnHL. These observations were taken together to build a novel mechanism of HABP1-mediated inhibition of SpnHL.

A Novel Mechanism for HABP1-mediated Inhibition of SpnHL—The fascinating aspect of our study is that the sugar is capable of binding to both enzyme and inhibitor, and in both cases, it is the β-1,4-glycosidic linkage of the sugar, which is buried in the receptors. Rationalization of the competitive nature of inhibition has further revealed that the enzyme SpnHL binds to the substrate and inhibitor in the same region, namely the active site cleft. It is remarkable that the doughnut-shaped HABP1 acting as an inhibitor uses only its negative face/side for blocking the enzyme, whereas the opposite side/face is used for binding to the relatively negatively charged HA. Evidently the inhibitor uses two distinct and spatially separate sites for binding to the enzyme and the substrate. Based on these observations from experiments as well as computational simulations, we hypothesize that HABP1 may use a novel and unique multipronged mechanism/model for lowering hyaluronidase activity. According to this model, on one hand, HABP1 obstructs the active site of the enzyme to inhibit its activity, thereby following the nature of competitive inhibition. On the other hand, it uses its large free side/face to bind and sequester up to three additional HA polymers from the matrix, thereby protecting HA from SpnHL-mediated degradation during infection. This model has been structurally depicted in Fig. 5. Although one of the three inter chain junctions (or HA binding sites) shows a slight loss of residue surface area during the inhibitory interaction, 21 of 24 residues depicted in Table 1 remain fully accessible and free to bind HA oligomers. Alternatively a single long polymer of HA may bind to HABP1 using all three of its binding sites to circumvent degradation.

Biological Implications—Our findings reveal that HABP1 interacts with and blocks a large number of crucial/conserved groups of residues in the active site cleft of SpnHL. A majority of bacterial hyaluronate lyases are known to have a high degree of sequence conservation in the cleft region, and consequently, we speculate that they may also be inhibited by HABP1 in a similar manner. In contrast, mammalian and bacteriophage hyaluronidase enzymes have very different sequence as well as structural
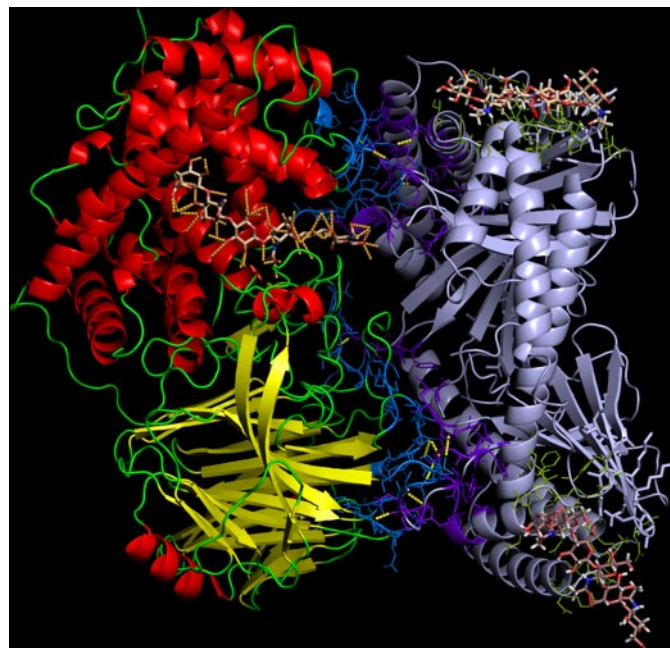

FIGURE 5. **Proposed model for the multifaceted mechanism of HABP1-mediated SpnHL inhibition.** In this figure, multiple HA hexasaccharide ligands (atom colors, *stick* representation) have been structurally superimposed upon the docked complex of enzyme and inhibitor (trimer shown in *gray*). SpnHL has been colored by secondary structure (helices, *red*; *sheets*, yellow; *loops*, green), and its active site has been depicted with HA oligomer to highlight how the substrate binding region is entirely blocked by the one side/face of the inhibitor. Similarly multiple HA oligomers have been depicted bound to the inhibitor to show that the three HA binding motif sites (*green*, *line* representation) are free to bind substrate HA molecules even when one entire side of the protein is blocking the SpnHL active site. Residues of the enzyme and inhibitor within 5 Å of each other are depicted in *blue* and *purple lines*. Hydrogen bonds are depicted as *yellow dashes*. The HA orientations used for superimposition have been taken from the crystal structure (for SpnHL), and the top ranking docked complexes are discussed in the text (for HABP1).

architectures and are therefore not likely to be inhibited by HABP1. It may be conjectured that this strategy of selective defense against bacterial hyaluronidases may have evolved in mammalian hosts to protect their own hyaluronidases from inhibition. It is encouraging to note that there have been reports of up-regulation and involvement of HABP1 in inflammation, apoptosis, and bacterial infections like *Listeria* (44, 45). Based on the crystal structure it has been suggested that terminal α-helices of HABP1 are critical for maintaining trimeric assembly as well as protein-protein interactions (33, 46). This is also evident from the Trp-Glu signature motif at the N-terminal region of HABP1 that is homologous to the WD-40 family of proteins that play predominant roles in interprotein interactions (47). A few viral proteins and bacterial proteins have already been reported to interact with HABP1 (48). However, although its multifunctional nature has been characterized, its role in hyaluronan protection has never been explored before.

Apart from the ability to competitively inhibit bacterial hyaluronidases, HABP1 has the added advantage of being able to bind and sequester multiple HA oligomers by virtue of its unique structural asymmetry. Our observations thus also explain the inherent charge asymmetry of the HABP1 structure that had not been accounted for until now. It may be speculated that, at least to some extent, this characteristic may be used to

protect the host HA matrix from endogenous hyaluronidases as well.

Competitive inhibition conventionally refers to structural analogy between substrate and inhibitor leading to competition of both for the active site of the enzyme. It must be noted that although we demonstrate the phenomenon of competitive inhibition here the inhibitor is structurally distinct from the substrate, and there is also a simultaneous blocking interaction of HABP1 with its substrate HA. Such a dual mode of inhibition is a unique phenomenon by itself, not previously demonstrated by any other enzyme inhibitor. It is true that free unbridled hyaluronidase activity would create much havoc, and nature must have created a great number of mechanisms for keeping these enzymes in check, mechanisms that must function at multiple levels. We believe that the data presented in this work may describe how remarkable such checking mechanisms can be and that they may indeed function at multiple levels simultaneously.

In conclusion, the identification of HABP1 as a competitive inhibitor of SpnHL constitutes a new line of defense against bacterial invasion and offers novel opportunities for therapeutic intervention, making it a highly suitable candidate to be investigated further for optimization of potency and specificity against bacterial virulence factors. Furthermore based on the insights obtained in this study, it will be possible to design short inhibitory peptides for binding and protecting HA polymers. Efforts in this direction present an alternative to synthetic chemicals and are currently underway in our laboratory.

REFERENCES

1. Chain, E., and Duthie, E. S. (1939) *Nature* **144,** 977–978
2. Mathews, M. B., and Dorfman, A. (1955) *Physiol. Rev.* **35,** 381–402
3. Hynes, W. L., and Walton, S. L. (2000) *FEMS Microbiol. Lett.* **183,** 201–207
4. Rapport, M. M., Linker, A., and Meyer, K. (1951) *J. Biol. Chem.* **192,** 283–291
5. Laurent, T. C., Laurent, U. B., and Fraser, J. R. (1996) *Immunol. Cell Biol.* **74,** A1–7
6. Day, T. D. (1950) *Nature* **166,** 785–786
7. Csoka, T. B., Frost, G. I., and Stern, R. (1997) *Invasion Metastasis* **17,** 297–311
8. Weissmann, B., Meyer, K., Sampson, P., and Linker, A. (1954) *J. Biol. Chem.* **208,** 417–429
9. Kreil, G. (1995) *Protein Sci.* **4,** 1666–1669
10. Jedrzejas, M. J., Mewbourne, R. B., Chantalat, L., and McPherson, D. T. (1998) *Protein Expr. Purif.* **13,** 83–89
11. Li, S., Kelly, S. J., Lamani, E., Ferraroni, M., and Jedrzejas, M. J. (2000) *EMBO J.* **19,** 1228–1240
12. Laurent, T. C., and Fraser, J. R. (1992) *FASEB J.* **6,** 2397–2404
13. Stern, R. (2004) *Eur. J. Cell Biol.* **83,** 317–325
14. Stern, R. (2003) *Glycobiology* **13,** 105R–115R
15. Meyer, K., and Rapport, M. M. (1951) *J. Biol. Chem.* **188,** 485–490
16. Haas, E. (1946) *J. Biol. Chem.* **163,** 63–68
17. Fiszer-Szafarz, B. (1968) *Proc. Soc. Exp. Biol. Med.* **129,** 300–302
18. Dorfman, A., Ott, M. L., and Whitney, R. (1948) *J. Biol. Chem.* **174,** 621–629
19. Brodiagin, N. A., and Saburov, G. E. (1970) *Biull. Eksp. Biol. Med.* **70,** 52–54
20. Asada, M., Sugie, M., Inoue, M., Nakagomi, K., Hongo, S., Murata, K., Irie, S., Takeuchi, T., Tomizuka, N., and Oka, S. (1997) *Biosci. Biotechnol. Biochem.* **61,** 1030–1032
21. Kuppusamy, U. R., Khoo, H. E., and Das, N. P. (1990) *Biochem. Pharmacol.* **40,** 397–401
22. Mio, K., Csoka, A. B., Nawy, S. S., and Stern, R. (2001) *Methods Mol. Biol.* **171,** 391–397
23. Udabage, L., Brownlee, G. R., Stern, R., and Brown, T. J. (2004) *Glycoconj. J.* **20,** 461–471
24. Li, S., Taylor, K. B., Kelly, S. J., and Jedrzejas, M. J. (2001) *J. Biol. Chem.* **276,** 15125–15130
25. Spickenreither, M., Braun, S., Bernhardt, G., Dove, S., and Buschauer, A. (2006) *Bioorg. Med. Chem. Lett.* **16,** 5313–5316
26. Suzuki, K., Terasaki, Y., and Uyeda, M. (2002) *J. Enzyme Inhib. Med. Chem.* **17,** 183–186
27. Botzki, A., Rigden, D. J., Braun, S., Nukui, M., Salmen, S., Hoechstetter, J., Bernhardt, G., Dove, S., Jedrzejas, M. J., and Buschauer, A. (2004) *J. Biol. Chem.* **279,** 45990–45997
28. Turley, E. A., Noble, P. W., and Bourguignon, L. Y. (2002) *J. Biol. Chem.* **277,** 4589–4592
29. Toole, B. P. (1990) *Curr. Opin. Cell Biol.* **2,** 839–844
30. Day, A. J., and Prestwich, G. D. (2002) *J. Biol. Chem.* **277,** 4585–4588
31. Deb, T. B., and Datta, K. (1996) *J. Biol. Chem.* **271,** 2206–2212
32. Gupta, S., Batchu, R. B., and Datta, K. (1991) *Eur. J. Cell Biol.* **56,** 58–67
33. Jiang, J., Zhang, Y., Krainer, A. R., and Xu, R. M. (1999) *Proc. Natl. Acad. Sci. U. S. A.* **96,** 3572–3577
34. Jha, B. K., Salunke, D. M., and Datta, K. (2003) *J. Biol. Chem.* **278,** 27464–27472
35. Akhtar, M. S., and Bhakuni, V. (2003) *J. Biol. Chem.* **278,** 25509–25516
36. Yamagata, T., Saito, H., Habuchi, O., and Suzuki, S. (1968) *J. Biol. Chem.* **243,** 1523–1535
37. Jedrzejas, M. J., Mello, L. V., de Groot, B. L., and Li, S. (2002) *J. Biol. Chem.* **277,** 28287–28297
38. Hubbard, S. J., and Thornton, J. M. (1993) *NACCESS*, University College, London
39. Humphrey, W., Dalke, A., and Schulten, K. (1996) *J. Mol. Graph.* **14,** 33–38, 27–38
40. Delano, W. L. (2002) *The PyMOL User's Manual*, Delano Scientific, Palo Alto, CA
41. Yang, B., Yang, B. L., Savani, R. C., and Turley, E. A. (1994) *EMBO J.* **13,** 286–296
42. Deb, T. B., Majumdar, M., Bhardwaj, A., Jha, B. K., and Datta, K. (2001) in *Hyaluronan* (Kennedy, J. F., Philips, G. O., and Williams, P. A., eds) Vol. 1, pp. 365–372, Woodhead Publishing Ltd., Cambridge, UK
43. Rigden, D. J., Botzki, A., Nukui, M., Mewbourne, R. B., Lamani, E., Braun, S., von Angerer, E., Bernhardt, G., Dove, S., Buschauer, A., and Jedrzejas, M. J. (2006) *Glycobiology* **16,** 757–765
44. Ghebrehiwet, B., Lim, B. L., Kumar, R., Feng, X., and Peerschke, E. I. (2001) *Immunol. Rev.* **180,** 65–77
45. Braun, L., Ghebrehiwet, B., and Cossart, P. (2000) *EMBO J.* **19,** 1458–1466
46. Schaerer, M. T., Kannenberg, K., Hunziker, P., Baumann, S. W., and Sigel, E. (2001) *J. Biol. Chem.* **276,** 26597–26604
47. Iwasaki, Y., Komano, M., Ishikawa, A., Sasaki, T., and Asahi, T. (1995) *Plant Cell Physiol.* **36,** 505–510
48. Ito, S., Ikeda, M., Kato, N., Matsumoto, A., Ishikawa, Y., Kumakubo, S., and Yanagi, K. (2000) *Virology* **266,** 110–119